Formation of Highly Functionalized Metal-Bound Acetylenes by Reductive Coupling of Carbon Monoxide and Methyl Isocyanide Ligands

Edmund M. Carnahan and Stephen J. Lippard*

Contribution from the Department of Chemistry, Massachusetts Institute of Technology, Cambridge, Massachusetts 02139. *Received December 17, 1991*

Abstract: Reduction of $[M(CNMe)(CO)(dmpe)_2Cl]$ (M = Nb, Ta; dmpe = 1,2-bis(dimethylphosphino)ethane) with 40% Na/Hg followed by addition of Me_3SiCl achieved the reductive coupling of the CO and CNMe ligands to form $[M\{(Me_3Si)(Me)NC{\equiv}CO(SiMe_3)\}(dmpe)_2Cl]$. The niobium complex was characterized in a single-crystal X-ray diffraction study, which revealed the presence of the unprecedented RR'NC≡COR acetylene ligand. The reductive coupling reaction proceeds by a mechanism analogous to that previously reported for the symmetric coupling of two carbon monoxide or two alkyl isocyanide ligands. The first step in the reaction is the formation of an aminocarbyne intermediate, a triphenylsilyl derivative of which was crystallographically characterized. Addition of Me_3SiCl to $[Nb\{CN(Me)(SiMe_2Bu^t)\}(CO)(dmpe)_2]$ generated the asymmetric coupled product, $[Nb\{(^tBuMe_2Si)(Me)NC{\equiv}CO(SiMe_3)\}(dmpe)_2Cl]$, demonstrating that aminocarbyne complexes are on the mechanistic pathway to reductive coupling. Addition of aqueous acid to $[Ta\{(Me_3Si)(Me)NC{\equiv}CO(SiMe_3)\}(dmpe)_2Cl]$ provided the first stabilized hydroxy(alkylamino)acetylene complex, $[TaH(MeHNC{\equiv}COH)(dmpe)_2Cl]Cl$, a compound that was also crystallographically characterized. Finally, reductive coupling of two isocyanide ligands in $[Ta(CNMe)_2(dmpe)_2Cl]$ has been accomplished, demonstrating that all three possible combinations of CO and CNR ligands can be reductively coupled in reactions that use the same metal framework and generalized mechanism.

Introduction

Reactions that convert inexpensive feedstock chemicals such as carbon monoxide into functionalized polycarbon compounds are of considerable current interest.[1-5] Classical Fischer–Tropsch chemistry achieves this transformation efficiently, but without a high degree of product selectivity. For this reason, much research has been devoted to the development of homogeneous systems that selectively link CO and other C_1 fragments.[6-10]

Studies in our laboratory have concentrated on reactions that lead to the reductive coupling of two adjacent carbon monoxide[11-13] or alkyl isocyanide[14-16] ligands in low-valent, early transition metal complexes. These transformations are depicted in eqs 1 and 2, respectively, where two adjacent CO or CNR ligands are converted into a bound acetylene fragment in a series of discrete, well-defined reactions (Scheme I).[11,17-19] In the first step, a seven-coordinate d⁴ complex is reduced with loss of a capping halide ligand to generate an electron-rich, d⁶ octahedral species. These electron-rich reduced complexes are susceptible to electrophilic attack at the heteroatom of the ligand, and addition of a single equivalent of EX gives a substituted carbyne complex. Addition of a second equivalent of EX induces CO- or CNR–carbyne coupling to form the final acetylene moiety (Scheme I).

Scheme I. General Reaction Scheme for Reductive Coupling of Two Carbonyl or Alkyl Isocyanide Ligands

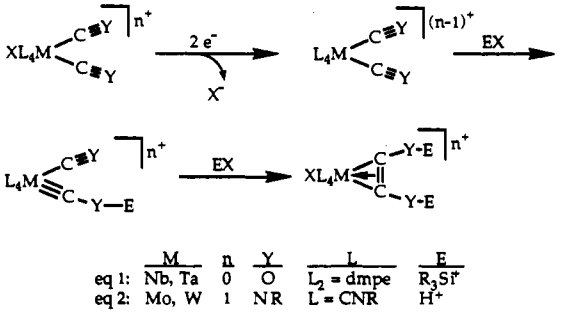

	M	n	Y	L	E
eq 1:	Nb, Ta	0	O	L_2 = dmpe	R_3Si^+
eq 2:	Mo, W	1	NR	L = CNR	H^+

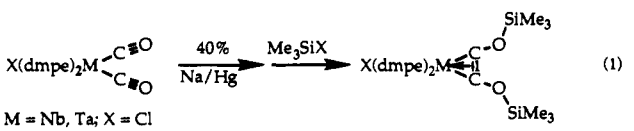

(1)

M = Nb, Ta; X = Cl

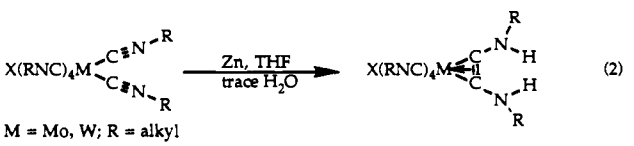

(2)

M = Mo, W; R = alkyl
X = halide, CN^-

The resulting η^2-coordinated acetylene can undergo further derivatization. For example, addition of aqueous acid to $[Ta(Me_3SiOCCOSiMe_3)(dmpe)_2Cl]$ affords $[TaH(HOCCOH)(dmpe)_2Cl]Cl$, the first metal dihydroxyacetylene complex.[20] In

(1) Whyman, R.; Gilhooley, K.; Rigby, S.; Winstanley, D. In *Industrial Chemicals via C_1 Processes*; Fahey, D. R., Ed.; American Chemical Society: Washington, DC, 1987; p 108.
(2) Sheldon, R. A. *Chemicals from Synthesis Gas*; D. Reidel Publishing Company: Dordrecht, Holland, 1983, p 185 ff.
(3) Herrmann, W. A. *Angew. Chem., Int. Ed. Engl.* **1982**, *21*, 117.
(4) Frohning, C. D. In *New Synthesis with Carbon Monoxide*; Falbe, J., Ed.; Springer-Verlag: Berlin, 1980; p 320 ff.
(5) Masters, C. *Adv. Organomet. Chem.* **1979**, *17*, 61.
(6) Mayr, A.; Bastos, C. M. *Prog. Inorg. Chem.*, in press.
(7) Carnahan, E. M.; Protasiewicz, J. D.; Lippard, S. J. To be submitted for publication.
(8) Vrtis, R. N.; Lippard, S. J. *Isr. J. Chem.* **1990**, *30*, 331.
(9) Templeton, J. L. *Adv. Organomet. Chem.* **1989**, *29*, 1.
(10) Kahn, B. E.; Rieke, R. D. *Chem. Rev.* **1988**, *88*, 733.
(11) Vrtis, R. N.; Liu, S.; Rao, C. P.; Bott, S. G.; Lippard, S. J. *Organometallics* **1991**, *10*, 275.
(12) Bianconi, P. A.; Vrtis, R. N.; Rao, C. P.; Williams, I. D.; Engeler, M. P.; Lippard, S. J. *Organometallics* **1987**, *6*, 1968.
(13) Bianconi, P. A.; Williams, I. D.; Engeler, M. P.; Lippard, S. J. *J. Am. Chem. Soc.* **1986**, *108*, 311.
(14) Warner, S.; Lippard, S. J. *Organometallics* **1986**, *5*, 1716.
(15) Giandomenico, C. M.; Lam, C. T.; Lippard, S. J. *J. Am. Chem. Soc.* **1982**, *104*, 1263.
(16) Lam, C. T.; Corfield, P. W. R.; Lippard, S. J. *J. Am. Chem. Soc.* **1977**, *99*, 617.
(17) Carnahan, E. M.; Lippard, S. J. *J. Chem. Soc., Dalton Trans.* **1991**, 699.
(18) Vrtis, R. N.; Rao, C. P.; Lippard, S. J. *J. Am. Chem. Soc.* **1988**, *110*, 2669.
(19) Filippou, A. C.; Grünleitner, W. *Z. Naturforsch., B* **1991**, *46*, 216.
(20) Vrtis, R. N.; Bott, S. G.; Rardin, R. L.; Lippard, S. J. *Organometallics* **1991**, *10*, 1364.

0002-7863/92/1514-4166$03.00/0

contrast, the products of coupling reactions that occur at high-valent metallocene hydride and alkyl centers are less reactive,[10] because the heteroatoms of the coupled products are bound to an electron-deficient transition metal ion. Scheme I, therefore, outlines a unique pathway for the construction of highly-functionalized acetylene ligands from C_1 precursors.

An interesting extension of this chemistry is the cross-coupling of CO with CNR. Although there are now several examples of reductive coupling of two CO or two CNR ligands,[8-10] cross-coupling is rare. The $\{M(dmpe)_2Cl\}$ framework seemed to be well suited for achieving such a transformation, and synthetic routes to the $[M(CNR)(CO)(dmpe)_2Cl]$ starting materials were therefore developed.[21,22] Two reactions that utilize high-valent metal alkyl complexes to effect reductive coupling of CO with CNR ligands have been described. Addition of CNR′ to $[Zr(OAr)_2R_2]$ yielded the η^2-iminoacyl complex, $[Zr(R)(\eta^2\text{-}RCNR')(OAr)_2]$, which reacted further upon addition of CO to form the enamidolate metallocycle, $[Zr\{O(R)C{=}C(R)N(R')\}(OAr)_2]$.[23-26] Treatment of $[Cp^*_2Th(Cl)(CH_2R)]$ with 1 equiv each of CO and CNR′ afforded the ketenimine complex, $[Cp^*_2Th(Cl)\{O(CH_2R)C{=}C{=}NR'\}]$, by acyl–isocyanide coupling.[27] In contrast to these reactions, reductive coupling of CO with CNR by the route outlined in Scheme I would result in a functionalized acetylene moiety bound through both carbon atoms to the transition metal.

When $[Nb(CNMe)(CO)(dmpe)_2Cl]$ was subjected to the conditions outlined in eq 1, the reductively-coupled product $[Nb\{(Me_3Si)(Me)NC{\equiv}CO(SiMe_3)\}(dmpe)_2Cl]$ was obtained. This complex contains the (RR′NC≡COR) acetylene functionality, as previously communicated in preliminary form.[21] Here we present the mechanistic details of this chemistry, including the characterization of intermediates along the reaction pathway, and extension of the coupling to a tantalum analogue. Formation of the cross-coupled product is consistent with the reaction chemistry shown in Scheme I, which demonstrates the generality of the reaction mechanism. We also describe the further reaction of the coupled product to give the unprecedented hydroxy(methylamino)acetylene ligand, HOC≡CNHMe. Finally, use of the $\{Ta(dmpe)_2Cl\}$ system to couple two alkyl isocyanide ligands is presented, demonstrating that a single framework can be used to effect reductive coupling of CO and CNR in all three possible combinations.

Experimental Section

Chemicals and Instrumentation. Tetrahydrofuran (THF), diethyl ether, and pentane were distilled from sodium benzophenone ketyl under nitrogen. $[Nb(CNMe)(CO)(dmpe)_2Cl]$, $[Ta(CNMe)(CO)(dmpe)_2Cl]$, and $[Ta(CNMe)_2(dmpe)_2Cl]$ were synthesized as described elsewhere.[21,22] Forty percent Na/Hg was prepared according to a literature procedure.[28] Chlorotrimethylsilane (Me_3SiCl), chlorotriphenylsilane (Ph_3SiCl), and *tert*-butyldimethylsilyl chloride ($^tBuMe_2SiCl$) were purchased from commercial vendors and used without further purification. All experiments were carried out either in a nitrogen-filled Vacuum Atmospheres drybox or by conventional Schlenk line techniques under purified argon. Infrared spectra were recorded on Mattson Cygnus 100 or BioRad FTS7 Fourier transform instruments. NMR spectra were obtained by using Varian Gemini-300 or Varian XL-300 spectrometers. ^1H NMR chemical shifts were obtained by comparison to residual solvent proton positions, and ^{31}P NMR spectra were obtained by comparison to an external 85% H_3PO_4 sample. X-ray crystal structure data were collected by previously reported methods.[22,29]

Preparation of $[Nb\{(Me_3Si)(Me)NC{\equiv}CO(SiMe_3)\}(dmpe)_2Cl]$ (1a). The compound $[Nb(CNMe)(CO)(dmpe)_2Cl]$ (0.067 g, 0.135 mmol) was dissolved in 10 mL of THF. Excess 40% Na/Hg was added to the red solution and the mixture was stirred for 30 min. The resulting dark violet solution was decanted, and 35 μL of $[Me_3SiCl]$ (0.276 mmol) was added. The solution slowly turned green over a 30-min period. The solvent was removed in vacuo and the residue extracted into 5 mL of pentane. Filtration and solvent removal afforded **1a** in quantitative yield. The green solid was extracted into ~2 mL of pentane and chilled to −30 °C to produce 0.059 g (68%) of **1a** as dark green crystals. IR (KBr): 2960 (m), 2897 (s), 2802 (w), 1550 (s), 1420 (m), 1396 (w), 1243 (s), 1147 (s), 1086 (m), 1003 (m), 935 (s), 889 (s), 846 (s), 752 (m), 718 (m), 680 (m), 611 (m), 447 (w) cm^{-1}. ^1H NMR (300 MHz, C_6D_6): δ 3.26 (3 H, N*Me*), 1.65 (br, 4 H, P*CH*$_2$), 1.58 (br, 12 H, P*CH*$_3$), 1.22 (br, 12 H, P*CH*$_3$), 1.13 (br, 4 H, P*CH*$_2$), 0.46 (9 H, Si*Me*$_3$), 0.19 (9 H, Si*Me*$_3$) ppm. $^{31}P\{^1H\}$ NMR (121 MHz, C_6D_6): 35 (v br, unresolved Nb–P coupling) ppm. Anal. Calcd for $C_{21}H_{53}ClNNbOP_4Si_2$ (**1a**): C, 39.16; H, 8.29; N, 2.17. Found: C, 39.31; H, 7.67; N, 2.41.

Preparation of $[Ta\{(Me_3Si)(Me)NC{\equiv}CO(SiMe_3)\}(dmpe)_2Cl]$ (1b). Preparation of **1b** followed the same procedure used for the synthesis of **1a**. Addition of an excess of 40% Na/Hg to a THF solution of 0.058 g of $[Ta(CNMe)(CO)(dmpe)_2Cl]$ (0.099 mmol) caused a color change from red to dark red-brown. After 45 min the solution was decanted from the amalgam and 26 μL of $[Me_3SiCl]$ (0.205 mmol) was added. The reaction mixture slowly turned green over a 30-min period. Workup as described above for **1a** yielded 0.066 g (91%) of **1b** as a dark green solid. Recrystallization from pentane at −30 °C yielded 0.046 g (63%) of **1b** as large, green crystals. IR (KBr): 2958 (w), 2894 (m), 1544 (s), 1419 (m), 1243 (m), 1145 (w), 1091 (m), 932 (m), 901 (m), 885 (m), 845 (s), 680 (m), 608 (w) cm^{-1}. ^1H NMR (300 MHz, C_6D_6): 3.14 (3 H, N*Me*), 1.78 (br, 4 H, P*CH*$_2$), 1.63 (m, J_{P-H} = 1.8 Hz, additional coupling unresolved, 12 H, P*CH*$_3$), 1.28 (m, J_{P-H} = 1.8 Hz, additional coupling unresolved, 12 H, P*CH*$_3$), 1.14 (br, 4 H, P*CH*$_2$), 0.42 (9 H, Si*Me*$_3$), 0.20 (9 H, Si*Me*$_3$). $^{31}P\{^1H\}$ NMR (121 MHz, C_6D_6): 26.69 ppm. Anal. Calcd for $C_{21}H_{53}ClNOP_4Si_2Ta$ (**1b**): C, 34.45; H, 7.30; N, 1.91; P, 16.92. Found: C, 34.07; H, 7.10; N, 1.86; P, 17.33.

Reduction of $[M(CNMe)(CO)(dmpe)_2Cl]$ To Form $Na[M(CNMe)(CO)(dmpe)_2]$, M = Nb (2a), Ta (2b). $[M(CNMe)(CO)(dmpe)_2Cl]$ (0.05 g) was dissolved in 10 mL of THF and a >100-fold excess of 40% Na/Hg was added. After 30 min, the dark violet (M = Nb) or red-brown (M = Ta) solution was filtered and the solvent removed to yield a red-brown solid. Spectroscopic characterization was consistent with the formation of $Na[Nb(CNMe)(CO)(dmpe)_2]$ (**2a**) and $Na[Ta(CNMe)(CO)(dmpe)_2]$ (**2b**), respectively. Spectroscopic data for **2a** were as follows: IR (KBr): 2920 (m), 2895 (s), 2832 (w), 1610 (s), 1540 (s), 1415 (m), 1370 (s), 1290 (m), 1281 (m), 935 (s), 876 (m), 650 (w), 608 (m) cm^{-1}. ^1H NMR (236 K, 300 MHz, THF-d_8): 2.74 (N*CH*$_3$), 1.52 (d, J_{P-H} = 5.1 Hz, P*CH*$_3$), 1.47 (d, J_{P-H} = 3.0 Hz, P*CH*$_3$), 1.39 (d, J_{P-H} = 1.8 Hz, P*CH*$_3$), 1.36 (d, J_{P-H} = 1.8 Hz, P*CH*$_3$), 1.30 (t, J_{P-H} = 3.6 Hz, P*CH*$_3$), 1.06 (br, P*CH*$_3$), 1.02 (br, P*CH*$_3$), 0.97 (d, J_{P-H} = 1.8 Hz, P*CH*$_3$) ppm. The dmpe methylene ^1H NMR resonances were obscured by the methyl signals. $^{31}P\{^1H\}$ NMR (236 K, 121 MHz, THF-d_8): 37.4, 31.3, 19.1, 14.2 ppm. Spectroscopic data for **2b** were as follows. IR (KBr): 2970 (m), 2924 (s), 2864 (w), 1614 (s), 1540 (s), 1416 (m), 1364 (s), 1310 (w), 928 (s), 901 (m), 879 (w), 680 (m) cm^{-1}. ^1H NMR (300 MHz, THF-d_8): 2.77 (N*CH*$_3$), 1.7–1.3 (br, P*CH*$_3$ and P*CH*$_2$), 1.13 (br, P*CH*$_3$), 1.09 (br, P*CH*$_3$), 0.96 (t, J_{P-H} = 1.8 Hz, P*CH*$_3$) ppm. $^{31}P\{^1H\}$ NMR (121 MHz, THF-d_8): 23.9, 21.2, 9.7, 4.9 ppm. Addition of 2 $[Me_3SiCl]$ to the NMR sample of **2b** indicated complete conversion to **1b** by $^{31}P\{^1H\}$ NMR spectroscopy.

Preparation of $[Nb\{CN(Me)(SiPh_3)\}(CO)(dmpe)_2]$ (3a). To a solution of 0.050 g of $[Nb(CNMe)(CO)(dmpe)_2Cl]$ (0.10 mmol) in 10 mL of THF was added an excess of 40% Na/Hg as described for the synthesis of **2a**. After 30 min, the dark violet solution was decanted, and 0.030 g of Ph_3SiCl (0.10 mmol) in 3 mL of THF was added. The violet solution turned deep red over a 30-min period. The solvent was removed and the residue extracted into 10 mL of pentane. Removal of solvent yielded 0.071 g of **3a** as an orange-red microcrystalline solid (98% yield). The product was dissolved in ~3 mL of Et_2O and cooled to −30 °C to yield large red crystals of **3a**·$^1/_2Et_2O$, which were dried under vacuum. Yield was 0.046 g (64% based on niobium). IR (KBr): 3067 (w), 3048 (w), 2960 (w), 2891 (m), 1751 (s), 1419 (m), 1261 (s), 1112 (m), 932 (m), 769 (m), 711 (s), 699 (s), 629 (w), 525 (m), 516 (m), 501 (w), 497 (w) cm^{-1}. Preparation of **3a** from $[Nb(^{13}CO)(CNMe)(dmpe)_2Cl]$[22] resulted in a shift of the 1751-cm^{-1} band to 1716 cm^{-1}. ^1H NMR (300 MHz, C_6D_6): 8.48 (m, 6 H, C_6H_5), 7.34–7.20 (m, 9 H, C_6H_5), 3.18 (3 H, N*CH*$_3$), 1.58 (d, J_{P-H} = 6.0 Hz, 3 H, P*CH*$_3$), 1.43 (d, J_{P-H} = 5.4 Hz,

(21) Carnahan, E. M.; Lippard, S. J. *J. Am. Chem. Soc.* **1990**, *112*, 3230.
(22) Carnahan, E. M.; Rardin, R. L.; Bott, S. G.; Lippard, S. J. To be submitted for publication.
(23) Durfee, L. D.; Rothwell, I. P. *Chem. Rev.* **1988**, *88*, 1059.
(24) Chamberlain, L. R.; Durfee, L. D.; Fanwick, P. E.; Kobriger, L. M.; Latesky, S. L.; McMullen, A. K.; Steffey, B. D.; Rothwell, I. P.; Folting, K.; Huffman, J. C. *J. Am. Chem. Soc.* **1987**, *109*, 6068.
(25) Latesky, S. J.; McMullen, A. K.; Niccolai, G. P.; Rothwell, I. P.; Huffman, J. C. *Organometallics* **1985**, *4*, 1896.
(26) McMullen, A. K.; Rothwell, I. P.; Huffman, J. C. *J. Am. Chem. Soc.* **1985**, *107*, 1072.
(27) Moloy, K. G.; Fagan, P. J.; Manriquez, J. M.; Marks, T. J. *J. Am. Chem. Soc.* **1986**, *108*, 56.
(28) Fieser, L. F.; Fieser, M. *Reagents for Organic Synthesis*; Wiley: New York, 1967; Vol. 1, p 1033.
(29) Silverman, L. D.; Dewan, J. C.; Giandomenico, C. M.; Lippard, S. J. *Inorg. Chem.* **1980**, *19*, 3379.

Table I. X-ray Crystal Structure Data Collection Parameters[a] for [Nb{(Me$_3$Si)(Me)NC≡CO(SiMe$_3$)}(dmpe)$_2$Cl] (**1a**), [Nb{CN(Me)(SiPh$_3$)}(CO)(dmpe)$_2$]·$^1/_2$Et$_2$O (**3a**·$^1/_2$Et$_2$O), [Nb{('BuMe$_2$Si)(Me)NC≡CO(SiMe$_3$)}(dmpe)$_2$Cl] (**4**), and [TaH(HOC≡CNHMe)(dmpe)$_2$Cl]Cl·CHCl$_3$ (**5**·CHCl$_3$)

	1a	**3a**·$^1/_2$Et$_2$O	**4**	**5**·CHCl$_3$
a, Å	10.204 (5)	13.340 (4)	11.331 (1)	8.589 (2)
b, Å	18.475 (1)	17.694 (1)	17.293 (2)	13.017 (3)
c, Å	9.776 (5)	17.458 (7)	36.786 (7)	26.218 (5)
β, deg	115.51 (2)	108.03 (1)	93.17 (1)	
V, Å^3	1663 (1)	3918 (2)	7197 (1)	2193 (1)
temp, °C	−50	−78	−78	−78
fw, g mol^{-1}	644.08	758.72	686.15	743.60
Z	2	4	8	4
ρ_{calc}, g cm^{-3}	1.29	1.29	1.27	1.68
space group	$P2_1$ (No. 4)	$P2_1/n$ (No. 14)	$P2_1/n$ (No. 14)	*Pnma* (No. 62)
2 θ limits	$3 \le 2\theta \le 50$	$3 \le 2\theta \le 46$	$3 \le 2\theta \le 48$	$3 \le 2\theta \le 50$
data limits	$+h +k \pm l$	$\pm h +k +l$	$\pm h +k +l$	$+h +k +l$
crystal dim, mm	0.20 × 0.23 × 0.38	0.15 × 0.20 × 0.25	0.18 × 0.28 × 0.45	0.07 × 0.10 × 0.33
μ, cm^{-1}	7.02	5.12	6.52	43.9
transmission factors	0.78–0.89	0.89–1.00	0.81–0.94	0.63–0.74
total data	4124	6262	12084	3086
unique data	3077	5674	11694	2969
$R_{(merge)}$[b]	0.020	0.033	0.028	0.038
unique obsd[c]	2780	3598	6536	1637
no. of LS parameters	279	424	630	141
p factor	0.05	0.05	0.05	0.07
R[d]	0.034	0.055	0.055	0.065
R_w	0.042	0.076	0.072	0.088

[a] Data collected on an Enraf Nonius CAD-4F kappa geometry diffractometer using Mo Kα radiation. [b] $R_{(merge)} = \sum_{i=1}^{n}\sum_{j=1}^{m}|\langle F_i^2\rangle - F_{ij}^2|/\sum_{i=1}^{n} m \times \langle F_i^2\rangle$ where n = number unique reflections observed more than once, m = number of times a given reflection is observed, and $\langle F_i^2\rangle$ is the average value of F^2 for reflection i. [c] Observation criterion $I > 3\sigma(I)$. [d] $R = \sum||F_o| - |F_c||/\sum|F_o|$, $R_w = [\sum w(|F_o| - |F_c|)^2/\sum w|F_o|^2]^{1/2}$, where $w = 1/\sigma^2(F)$.

3 H, PC*H*$_3$), 1.23 (d, J_{P-H} = 4.5 Hz, 3 H, PC*H*$_3$), 1.17 (d, J_{P-H} = 5.4 Hz, 3 H, PC*H*$_3$), 1.12 (d, J_{P-H} = 6.6 Hz, 3 H, PC*H*$_3$), 0.96 (d, J_{P-H} = 3.3 Hz, 3 H, PC*H*$_3$), 0.89 (d, J_{P-H} = 3.3 Hz, 3 H, PC*H*$_3$), 0.54 (d, J_{P-H} = 2.4 Hz, 3 H, PC*H*$_3$) ppm. The dmpe methylene resonances appeared as broad signals from 1.6 to 1.0 ppm and were obscured by the methyl proton resonances. Anal. Calcd for $C_{33}H_{50}NNbOP_4Si$ (**3a**): C, 54.92; H, 6.98; N, 1.94. Found: C, 55.15; H, 7.15; N, 1.45.

Preparation of [Nb{CN(Me)(SiMe$_2$Bu^t)}(CO)(dmpe)$_2$] (3b). To a solution of 0.075 g of [Nb(CNMe)(CO)(dmpe)$_2$Cl] (0.15 mmol) in 10 mL of THF was added an excess of 40% Na/Hg. After 30 min the dark violet solution was decanted from the amalgam, and 0.023 g of 'BuMe$_2$SiCl (0.15 mmol) was added. The solution quickly turned deep red. After 1 h the solvent was removed, and the residue was extracted into 5 mL of pentane. The solvent was removed in vacuo to yield **3b** as a red-brown viscous oil. Crude yield was 0.086 g (99% based on niobium). IR (KBr): 2954 (s), 2925 (s), 2894 (s), 2853 (m), 1773 (m), 1471 (w), 1420 (m), 1291 (m), 1269 (m), 1120 (w), 932 (s), 892 (s), 738 (m), 708 (w), 684 (w) cm^{-1}. ^{1}H NMR (293 K, 300 MHz, C_6D_6): 3.00 (3 H, NC*H*$_3$), 1.75 (d, J_{P-H} = 6.0 Hz, 3 H, PC*H*$_3$), 1.64 (d, J_{P-H} = 6.0 Hz, 3 H, PC*H*$_3$), 1.35 (m, 6 H, overlapping PC*H*$_3$), 1.21 (d, J_{P-H} = 4.0 Hz, 3 H, PC*H*$_3$), 1.08 (br, 12 H, overlapping PC*H*$_3$ and Si*Bu^t*), 0.94 (br, 3 H, PC*H*$_3$), 0.62 (br, 3 H, PC*H*$_3$), 0.36 (3 H, SiC*H*$_3$), 0.29 (3 H, SiC*H*$_3$) ppm. The dmpe methylene resonances appeared as broad signals from 1.6 to 0.8 ppm and were obscured by the methyl proton signals. Although **3b** was the only niobium-containing product observed by NMR spectroscopy, it could not be crystallized to obtain analytically pure material.

Preparation of [Nb{('BuMe$_2$Si)(Me)NC≡CO(SiMe$_3$)}(dmpe)$_2$Cl] (4). To 0.086 g of [Nb{CN(Me)(SiMe$_2$Bu^t)}(CO)(dmpe)$_2$] (0.15 mmol) in 10 mL of THF was added 19 μL of Me$_3$SiCl (0.15 mmol). The solution slowly turned green-brown over a 30-min period. The solvent was removed in vacuo and the solid extracted into pentane. Chilling to −30 °C yielded 0.071 g (69%) of **4** as large green crystals. IR (KBr): 2957 (m), 2894 (s), 2853 (m), 1559 (s), 1469 (w), 1419 (m), 1245 (m), 1133 (s), 1076 (w), 992 (m), 931 (s), 900 (m), 874 (s), 860 (s), 697 (m), 682 (m), 610 (w) cm^{-1}. ^{1}H NMR (300 MHz, C_6D_6): 3.43 (3 H, NC*H*$_3$), 1.85 (4 H, br, PC*H*$_2$), 1.61 (12 H, PC*H*$_3$), 1.09 (16 H, overlapping PC*H*$_3$ and PC*H*$_2$), 0.98 (9 H, Si*Bu^t*), 0.51 (9 H, Si*Me*$_3$), 0.19 (6 H, Si*Me*$_2$) ppm. ^{31}P{^{1}H} NMR (121 MHz, C_6D_6): 32 ppm (v br, unresolved Nb–P coupling). Anal. Calcd for $C_{24}H_{59}NbClNOP_4Si_2$ (**4**): C, 42.01; H, 8.67; N, 2.04. Found: C, 42.23; H, 8.63; N, 2.17.

Preparation of [TaH(HOC≡CNHMe)(dmpe)$_2$Cl]Cl (5). To a solution of 0.080 g of [Ta{Me$_3$SiOC≡CN(Me)(SiMe$_3$)}(dmpe)$_2$Cl] (0.11 mmol) in 10 mL of THF was added 46 μL of oxygen-free 2.44 M HCl$_{aq}$ (0.11 mmol). The green solution immediately turned pale yellow. The solvent was removed and the product washed with two 10-mL portions of Et$_2$O. Extraction into 5 mL of CH$_2$Cl$_2$, filtration, and removal of solvent yielded 0.059 g (86% based on Ta) of [TaH(HOC≡CNHMe)(dmpe)$_2$Cl]Cl (**5**) as a white microcrystalline solid. IR (KBr): 3423 (w), 3323 (m), 2907 (m), 1622 (s), 1413 (s), 1291 (m), 1232 (m), 1047 (m), 932 (s), 900 (m), 713 (m), 650 (m), 597 (m), 551 (w) cm^{-1}. ^{1}H NMR (300 MHz, CD_2Cl_2): 10.52 (br, O*H*), 7.95 (v, br, N*H*), 5.14 (t of t, $J_{P-H\ trans}$ = 90 Hz, $J_{P-H\ cis}$ = 12 Hz, Ta–*H*), 3.10 (d, J_{H-H} = 2.1 Hz, NH*Me*), 2.1–1.9 (br, PC*H*$_2$), 1.70 (d, J_{P-H} = 7.4 Hz, PC*H*$_3$), 1.66 (d, J_{P-H} = 9.1 Hz, PC*H*$_3$), 1.60 (d, J_{P-H} = 7.8 Hz, PC*H*$_3$), 1.39 (d, J_{P-H} = 7.0 Hz, PC*H*$_3$) ppm. Addition of a small drop of D_2O to the sample caused the resonances at 10.52 and 7.95 ppm to disappear and the signal at 3.1 ppm to collapse to a singlet. The rest of the spectrum remained unchanged. ^{31}P{^{1}H} NMR (121 MHz, CD_2Cl_2): 35.2 (t, J_{P-P} = 25.7 Hz), 16.2 (t, J_{P-P} = 25.7 Hz) ppm. ^{31}P NMR (121 MHz, CD_2Cl_2): 35.2 (d, J_{P-H} = 82.9 Hz), 16.2 (br) ppm. Anal. Calcd for $C_{15}H_{38}Cl_2NOP_4Ta$ (**5**): C, 28.86; H, 6.14; N, 2.24. Found: C, 27.83; H, 6.18; N, 2.02.

Preparation of [Ta{(Me$_3$Si)(Me)NC≡CN(Me)(SiMe$_3$)}(dmpe)$_2$Cl] (6). To a solution of 0.112 g of [Ta(CNMe)$_2$(dmpe)$_2$Cl] (0.187 mmol) in 10 mL of THF was added an excess (>100-fold) of 40% Na/Hg. After 30 min, the solution had changed color from dark red to brown. The brown solution was decanted, and an excess (200 μL, 1.58 mmol) of Me$_3$SiCl was added. The solution was stirred for 12 h, after which time it was dark green. The solvent was removed in vacuo, and the yellow-green product was extracted into 5 mL of pentane. The solution was filtered and the solvent removed yielding 0.093 g (67% based on tantalum) of **6** as a pale yellow-green microcrystalline solid. IR (KBr): 2966 (m), 2894 (s), 1539 (m), 1419 (m), 1400 (m, sh), 1244 (m), 1090 (w), 1035 (w), 935 (s), 848 (s), 700 (w), 690 (w), 660 (w) cm^{-1}. ^{1}H NMR (300 MHz, C_6D_6): 3.02 (6 H, NC*H*$_3$), 1.83 (br, 4 H, PC*H*$_2$), 1.62 (12 H, PC*H*$_3$), 1.25 (12 H, PC*H*$_3$), 1.03 (br, 4 H, PC*H*$_2$), 0.22 (18 H, Si*Me*$_3$) ppm. ^{31}P{^{1}H} NMR (121 MHz, C_6D_6): 25.5 (br) ppm. Anal. Calcd for $C_{22}H_{56}ClN_2P_4Si_2Ta$: C, 35.46; H, 7.57; N, 3.76. Found: C, 35.03; H, 7.41; N, 3.70.

Collection and Reduction of X-ray Data. [Nb{(Me$_3$Si)(Me)NC≡CO(SiMe$_3$)}(dmpe)$_2$Cl] (1a). Green crystals of **1a** were obtained by slow cooling of a concentrated pentane solution to −20 °C. The crystals were transferred to a cold stage, and a single parallelepiped exhibiting {100}, {010}, and {001} forms was selected. The crystal was mounted on the tip of a fiber with silicone grease and transferred to the goniometer under a stream of cold nitrogen. Study on the diffractometer revealed a primitive monoclinic crystal system with the single absence $0k0$, $k \neq 2n$, consistent with the centrosymmetric $P2_1/m$ (C_{2h}^2, No. 11) and the noncentrosymmetric $P2_1$ (C_2^2, No. 4) space groups. The latter was selected based on better refinement and lower R values. The crystal was judged to be of acceptable quality based on open counter ω-scans of several strong, low-angle reflections ($\Delta\bar{\omega}_{1/2}$ = 0.30°, no fine structure) and axial photographs. An analytical absorption correction was applied to the data. Additional details may be found in Table I.

[Nb{CN(Me)(SiPh$_3$)}(CO)(dmpe)$_2$]·$^1/_2$Et$_2$O (3a·$^1/_2$Et$_2$O). Deep red crystals of **3a**·$^1/_2$Et$_2$O were grown from an ether solution at −40 °C. An

irregularly-shaped crystal was cut from a large plate and mounted as described above for **1a**. Study on the diffractometer revealed $2/m$ Laue symmetry with systematic absences $h0l$, $h + l \neq 2n$, and $0k0$, $k \neq 2n$, consistent with space group $P2_1/n$ (C_{2h}^5, No. 14, cell choice 2). Open counter ω-scans of several low-angle reflections ($\Delta\bar{\omega}_{1/2} = 0.32°$) revealed no fine structure. An empirical Ψ-scan correction was applied to the data. Additional details of data collection are given in Table I.

[Nb{('BuMe$_2$Si)(Me)NC≡CO(SiMe$_3$)}(dmpe)$_2$Cl] (4). Crystals of **4** were grown by slow cooling of a concentrated pentane solution to −30 °C. A single crystal with faces (101), (010), (011), (001), ($\bar{1}0\bar{1}$), ($0\bar{1}0$), and ($00\bar{1}$) was mounted as described above for **1a**. Study on the diffractometer indicated a primitive monoclinic crystal system with systematic absences $h0l$, $h + l \neq 2n$, and $0k0$, $k \neq 2n$, consistent with space group $P2_1/n$ (C_{2h}^5, No. 14, cell choice 2). The crystal was judged of acceptable quality based on open counter ω-scans of several strong, low-angle reflections ($\Delta\bar{\omega}_{1/2} = 0.27°$, no fine structure) and axial photographs. An analytical absorption correction was applied to the data. Additional details are given in Table I.

[TaH(HOC≡CNHMe)(dmpe)$_2$Cl]Cl·CHCl$_3$ (5·CHCl$_3$). Layering of pentane onto a chloroform solution of **5** yielded crystals of **5**·CHCl$_3$ as colorless rectangular plates. A single plate bound by {100}, {010}, and {001} was selected and mounted as described above for **1a**. Study on the diffractometer revealed *mmm* Laue symmetry with systematic absences $0kl$, $k + l \neq 2n$, and $hk0$, $h \neq 2n$, consistent with the centrosymmetric *Pnma* (D_{2h}^{16}, No. 62) and a nonconventional setting of the noncentrosymmetric *Pna*2$_1$ (C_{2v}^9, No. 33). The structure was solved and refined in the former space group, as described below. An analytical absorption correction was applied to the data. In addition, the data were corrected for a 12% isotropic decay. Additional details are given in Table I.

Structure Solution and Refinement

[Nb{(Me$_3$Si)(Me)NC≡CO(SiMe$_3$)}(dmpe)$_2$Cl] (1a). The niobium atom was located by direct methods and the rest of the non-hydrogen atoms were located by a series of least-squares refinements and difference Fourier maps. The methylene linker atoms for one dmpe chelate (C11 and C31) exhibited relatively large isotropic thermal parameters. Inspection of a difference Fourier map generated through a plane containing the two atoms failed to resolve any disorder, however, and these and all other non-hydrogen atoms were refined with anisotropic temperature factors. Hydrogen atoms were generated and fixed to "ride" at an average distance of 0.95 Å from the attached carbon atom (B_{iso} = 1.2B_{iso} carbon). Final refinement yielded the residuals given in Table I. Inversion of the coordinates and refinement of the other enantiomorph did not alter the *R* factors. The largest ratio of parameter shift to estimated standard deviation in the final cycles of refinement was found to be 0.057. The largest residual electron density found from the difference Fourier map was 0.50 e$^-$/Å^3 located near the niobium atom. Final atomic positional and anisotropic thermal parameters are given in Tables S1 and S2, respectively, and calculated and measured structure factors are given in Table S3.

[Nb{CN(Me)(SiPh$_3$)}(CO)(dmpe)$_2$]·$^1/_2$Et$_2$O (3a·$^1/_2$Et$_2$O). The niobium atom was located by direct methods, and all other non-hydrogen atoms were located by a series of least-squares refinements and difference Fourier maps. During refinement it became clear that the two dmpe chelate groups were disordered, corresponding to the two enantiomeric configurations of **3a**. This type of disorder has been resolved for a related vanadium siloxycarbyne species and reported previously;[30] it will therefore not be further discussed here. Atoms P2A, P4A, C2A1, and C4A1 were refined at 15% occupancy, while P2, P4, C21, and C41 were refined at 85% occupancy. All other atoms appeared at the same positions in both models and were refined at full occupancy. The methylene carbon atoms of one-half ether molecule in the asymmetric unit were also found to be disordered; atoms C101A and C101B were refined at half occupancy. Further details are available.[31] All non-hydrogen atoms except C2A1, C4A1, and C43, which were refined isotropically, were assigned anisotropic temperature parameters. Hydrogen atoms were treated as described above with the exception that no hydrogens were generated for disordered moieties. Final refinement yielded the residuals given in Table I. The largest shift/esd in the final cycles of refinement was found to be 0.01. The largest residual electron density found from the final difference Fourier map was 0.54 e$^-$/Å^3 and was located near the site of phosphine disorder. Final atomic positional and anisotropic thermal parameters for non-hydrogen atoms are given in Tables S4 and S5, respectively. Calculated and measured structure factors are given in Table S6.

(30) Protasiewicz, J. D.; Lippard, S. J. *J. Am. Chem. Soc.* **1991**, *113*, 6564.
(31) Carnahan, E. M. Ph.D. Thesis, Massachusetts Institute of Technology, 1991.

[Nb{('BuMe$_2$Si)(Me)NC≡CO(SiMe$_3$)}(dmpe)$_2$Cl] (4). Two independent molecules comprise the asymmetric unit. The niobium, phosphorus, and chlorine atoms were located by direct methods. Carbon and silicon atoms were found by subsequent least-squares refinements and difference Fourier syntheses. During refinement, an interesting disorder of the 'BuMe$_2$Si group was found in both molecules of the asymmetric unit. Two possible conformations of the ('BuMe$_2$Si) moiety of the {('BuMe$_2$Si)(Me)NC≡CO(SiMe$_3$)} ligand were present in 65:35 occupancy, as shown below. In the resulting model, atoms Si11, C116, and C119 were assigned 0.65 occupancy and Si11A, C116A, and C119A were assigned 0.35 occupancy (see Figure 4 for atom labeling scheme).

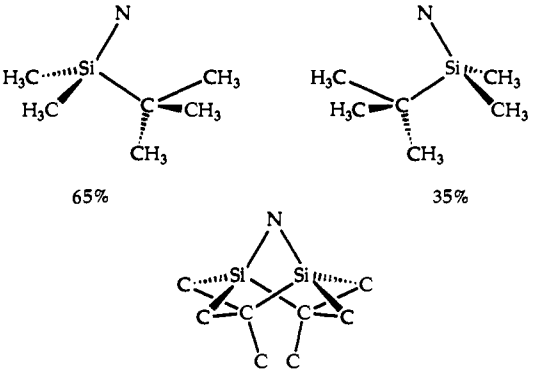

The remaining atoms of the group contribute to both conformations and were refined at full occupancy. Atoms in the second molecule of the asymmetric unit were treated in the same manner. In addition, C23 was disordered over three sites, each refined at 0.33 occupancy. All non-hydrogen atoms were refined with anisotropic temperature parameters except for the disordered carbon atoms. Hydrogen atoms were generated and treated as above except for those bonded to the carbon atoms involved in the disorder. Final refinement yielded the residuals given in Table I. The largest ratio of parameter shift to estimated standard deviation in the final cycles of refinement was 0.07. The largest residual electron density found from the difference Fourier map was 0.66 e$^-$/Å^3 and was located near a phosphorus atom. Final atomic positional and anisotropic thermal parameters for non-hydrogen atoms are given in Tables S7 and S8, respectively. Calculated and measured structure factors are given in Table S9.

[TaH(HOC≡CNHMe)(dmpe)$_2$Cl]Cl·CHCl$_3$ (5·CHCl$_3$). The position of the tantalum atom was determined by a Patterson synthesis, and the rest of the non-hydrogen atoms were determined by a series of least-squares refinements and difference Fourier maps. The structure was solved in the centrosymmetric space group *Pnma* with the tantalum, acetylene, and chloride counterion constrained to lie on a crystallographic mirror plane. The structure refined poorly because of a chloroform molecule in the lattice which was severely disordered across the mirror plane. Attempts to refine in the noncentrosymmetric space group *Pn*2$_1a$ gave significantly poorer results. The dmpe methylene linker atom C(21) was disordered across two sites with equal occupancy. Atom C(22) exhibited very large isotropic temperature factors, but no disorder of this atom could be resolved. No model was introduced to account for the chloroform disorder, and these and all other non-hydrogen atoms, with the exception of C(21) and C(21A), were assigned anisotropic temperature factors. Final refinement gave the residuals listed in Table I. The largest shift/esd in the final cycles of refinement was 0.05. A peak of 2.5 e$^-$/Å^3 was located very close to Cl(2) in the final difference map. This peak may result from site occupancy disorder of this counterion, although attempts to model it as such were unsuccessful. Final atomic positional and anisotropic thermal parameters for non-hydrogen atoms are given in Tables S10 and S11, respectively. Calculated and measured structure factors are given in Table S12.

Results and Discussion

Reductive Coupling of CO with CNMe. Reactions that reductively couple either two CO or two alkyl isocyanide ligands at seven-coordinate early transition metal centers proceed by analogous mechanisms (Scheme I).[11,17-19] It is therefore of interest to determine whether such a scheme can be further generalized to include other ligand combinations. As a first test of this principle, we investigated the cross coupling of CO with CNR, after having prepared the appropriate starting materials.[7,21] Reduction of [M(CNMe)(CO)(dmpe)$_2$Cl] (M = Nb, Ta) with 40% Na/Hg followed by addition of 2 equiv of Me$_3$SiCl generated the dark green [M{(Me$_3$Si)(Me)NC≡CO(SiMe$_3$)}(dmpe)$_2$Cl]

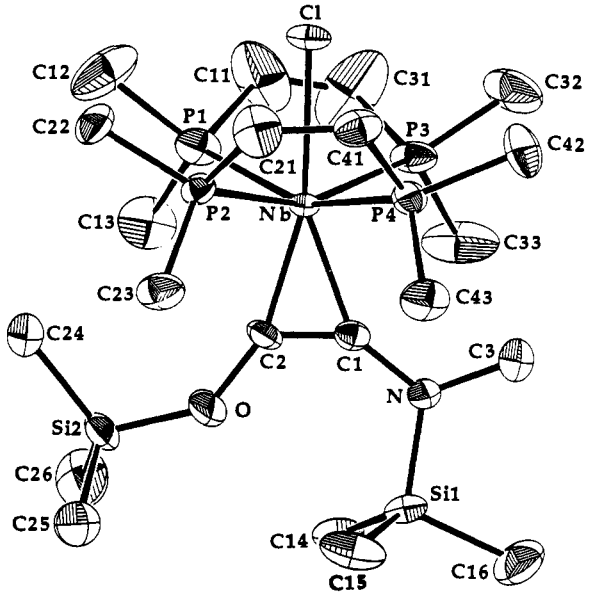

Figure 1. Structure of $[Nb\{(Me_3Si)(Me)NC{\equiv}CO(SiMe_3)\}(dmpe)_2Cl]$ (**1a**) showing the 40% probability thermal ellipsoids and the atom labeling scheme. Hydrogen atoms have been omitted.

(**1a**, M = Nb; **1b**, M = Ta) complexes in which adjacent C_1 ligands have been coupled (eq 3). The products exhibit no bands

$$[M(CNMe)(CO)(dmpe)_2Cl] \xrightarrow{40\%\ Na/Hg} \xrightarrow{2\ Me_3SiCl} [M\{(Me_3Si)(Me)NCCO(SiMe_3)\}(dmpe)_2Cl] \quad (3)$$
$$M = Nb,\ \mathbf{1a};\ M = Ta,\ \mathbf{1b}$$

assignable to C≡O or C≡NR stretches in the infrared spectrum, and their ^1H NMR spectra reveal two inequivalent trimethylsilyl groups and dmpe ligand proton resonances indicative of approximate mirror symmetry. These results are consistent with the formulation of **1a** and **1b** as seven-coordinate capped trigonal prismatic acetylene complexes, taking the coupled ligand as formally bidentate, analogous to the products formed from reductive coupling of two CO ligands.[12] An X-ray crystal structure determination of **1a** confirmed this assignment. An ORTEP diagram of this structure is shown in Figure 1, and a listing of bond distances and angles is given in Table II.

The planar acetylene ligand approximately bisects the pair of niobium–dmpe chelate rings. Several resonance forms can be written for the $Nb\{R_3SiOC{\equiv}CN(R)SiR_3\}$ moiety, as shown in the diagram below. The bond distances and angles support such

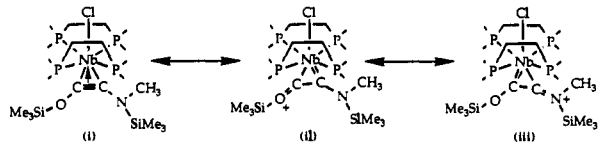

a delocalized electronic structure, with resonance form iii contributing most significantly to the bonding. The bond angles around the nitrogen atom are all ~120°, indicating sp^2-hybridization. In addition, the Nb–C2 bond is 0.05 Å shorter than that of Nb–C1. Although inter- and intramolecular packing forces might contribute to these inequivalences, close examination of space-filling models and packing diagrams did not reveal any such interactions.

The cross-coupling of CO with CNR represents a significant extension of the reductive coupling reaction. Although complexes containing symmetric ROC≡COR and RR'NC≡CNRR' acetylene ligands have been isolated previously,[9,12,13,15,16,30,32,33] to our knowledge **1a** and **1b** represent the first examples of

(32) H. G. Viehe, E. *Chemistry of Acetylenes*; Marcel Dekker: New York, 1969.

(33) Chisholm, M. H.; Ho, D.; Huffman, J. C.; Marchant, N. S. *Organometallics* **1989**, *8*, 1626.

Table II. Selected Bond Distances (Å) and Angles (deg) for $[Nb\{(Me_3Si)(Me)NC{\equiv}CO(SiMe_3)\}(dmpe)_2Cl]$ (**1a**)[a]

Coordination Sphere			
Bond Distances			
Nb–C(1)	2.125 (7)	Nb–P(3)	2.562 (2)
Nb–C(2)	2.079 (7)	Nb–P(4)	2.545 (2)
Nb–P(1)	2.573 (2)	Nb–Cl	2.586 (1)
Nb–P(2)	2.554 (2)		
Bond Angles			
C(1)–Nb–C(2)	35.9 (3)	P(1)–Nb–P(2)	98.74 (7)
C(1)–Nb–P(1)	116.2 (2)	P(1)–Nb–P(3)	76.93 (8)
C(1)–Nb–P(2)	112.5 (2)	P(1)–Nb–P(4)	157.53 (6)
C(1)–Nb–P(3)	88.2 (2)	P(1)–Nb–Cl	77.84 (6)
C(1)–Nb–P(4)	85.7 (2)	P(2)–Nb–P(3)	158.14 (6)
C(1)–Nb–Cl	159.1 (2)	P(2)–Nb–P(4)	75.47 (7)
C(2)–Nb–P(1)	93.0 (2)	P(2)–Nb–Cl	78.34 (5)
C(2)–Nb–P(2)	91.4 (2)	P(3)–Nb–P(4)	100.24 (8)
C(2)–Nb–P(3)	110.2 (2)	P(3)–Nb–Cl	79.80 (6)
C(2)–Nb–P(4)	108.6 (2)	P(4)–Nb–Cl	79.72 (6)
C(2)–Nb–Cl	164.9 (2)		
Ligand Geometry			
(i) Acetylene			
Bond Distances			
C(1)–C(2)	1.30 (1)	N–C(3)	1.47 (1)
C(1)–N	1.386 (9)	N–Si(1)	1.774 (6)
C(2)–O	1.385 (8)	O–Si(2)	1.615 (6)
mean Si–C	1.86 (1)	range Si–C	1.85–1.89
Bond Angles			
C(1)–C(2)–O	126.9 (7)	C(2)–C(1)–Nb	70.1 (5)
C(1)–N–C(3)	118.8 (6)	C(2)–O–Si(2)	140.3 (6)
C(1)–N–Si(1)	120.9 (5)	C(3)–N–Si(1)	119.5 (5)
C(2)–C(1)–N	140.4 (7)	N–C(1)–Nb	74.0 (4)
mean C–Si–C	109.5 (5)	range C–Si–C	107.0–112.8
(ii) 1,2-Bis(dimethylphosphine)ethane			
mean P–C	1.84 (1)	range P–C	1.81–1.88
mean C–P–C	100.2 (7)	range C–P–C	99.0–102.7

[a] Distances reported have not been corrected for thermal motion. Standard deviations quoted for the mean values are the average of the standard deviations for the individual values. See Figure 1 for atom-labeling scheme.

structures containing the asymmetric RR'NC≡COR ligand. Such an acetylene functionality was constructed at the metal center by designing a precursor that would couple the two C_1 ligands according to Scheme I. The strategy assumed that the mechanism for formation of **1a** and **1b** would be analogous to that found for the symmetric CO and CNR coupling reactions. Experiments that directly address this question are discussed next.

Mechanism of the Cross Coupling Reaction. Reduction of $[M(CNMe)(CO)(dmpe)_2Cl]$ to Form 2a, 2b. Reduction of $[M(CNMe)(CO)(dmpe)_2Cl]$ (M = Nb, Ta) complexes with 40% Na/Hg caused a color change from cherry red to very dark violet for **2a** and red-brown for **2b**. By analogy to the mechanism of reductive coupling of the two carbonyl ligands in $[M(CO)_2(dmpe)_2Cl]$ complexes,[11] we formulate these compounds as $Na[M(CNMe)(CO)(dmpe)_2]$ (eq 4). Efforts to purify these reactive

$$[M(CNMe)(CO)(dmpe)_2Cl] \xrightarrow{40\%\ Na/Hg} Na[M(CNMe)(CO)(dmpe)_2] \quad (4)$$
$$M = Nb,\ \mathbf{2a};\ M = Ta,\ \mathbf{2b}$$

intermediates by chromatography or counterion exchange were unsuccessful and led to decomposition. Spectroscopic characterization of the crude products, however, supports the proposed structural assignment. Both anions exhibit extremely low C≡O and C≡NR IR stretches (1610, 1540 cm^{-1} for **2a**, Figure 2; 1614, 1540 cm^{-1} for **2b**), which agree with those found for $Na[M(CO)_2(dmpe)_2]$ (M = V, Nb, Ta).[11,30] The $^{31}P\{^1H\}$ NMR spectra of **2a** (Figure 2) and **2b** display four broad resonances, consistent with a cis arrangement of isocyanide and carbonyl ligands. Addition of $[Me_3SiCl]$ to a THF-d_8 solution of **2b** rapidly gave the coupled product, **1b**, suggesting that the complex **2b** is a viable intermediate in the reductive coupling pathway.

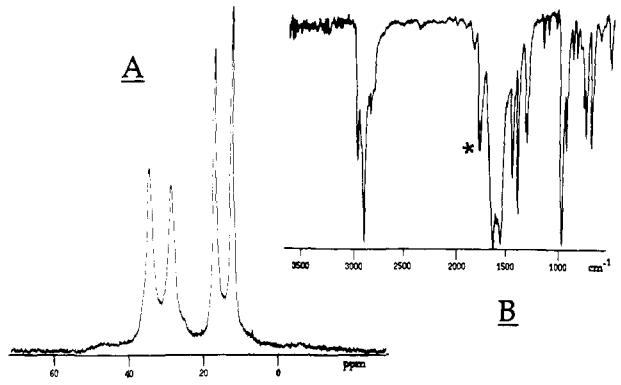

Figure 2. (A) $^{31}P\{^1H\}$ NMR spectrum of Na[Nb(CNMe)(CO)(dmpe)$_2$] (**2a**) in THF-d_8 at −40 °C. (B) IR spectrum of a KBr pellet of Na-[Nb(CNMe)(CO)(dmpe)$_2$] (**2a**). The peak marked with an asterisk arises from an impurity caused by oxidation of the sample.

The extreme reactivity of **2a** and **2b** was not unexpected, given the relatively poor π-acceptor properties of alkyl isocyanides as compared to carbonyl ligands. Whereas homoleptic, anionic carbonyl complexes are well-known, isocyanide analogues have only recently been prepared.[34] The [M(CO)$_5$(CNR)]$^-$ (M = V, Nb, Ta) anions,[35-37] formally isoelectronic with **2**, have C≡NR stretching frequencies that are typically greater than 2000 cm^{-1}, reflecting little transfer of electron density from the metal center to the isocyanide ligands. Substitution of the carbonyl groups by four phosphorus donors results in substantial transfer of metal π electron density to the C–N–C unit of the isocyanide ligand. The resulting [M(CNR)(CO)(dmpe)$_2$Cl] complexes contain strongly bent isocyanide ligands and C≡NR stretching frequencies ranging from 1775 to 1850 cm^{-1}.[22] Further reduction to form the anions **2a** and **2b** makes the isocyanide ligands extremely susceptible to electrophilic attack and the complexes easy to oxidize, accounting for the difficulty in isolating them in pure form.

Formation and Characterization of the Aminocarbyne Complex [Nb{≡CN(Me)(SiPh$_3$)}(CO)(dmpe)$_2$] (3a). The addition of 1 equiv of Ph$_3$SiCl to a THF solution of **2a** caused a subtle color change from dark violet to deep burgundy. After workup, **3a** was isolated as a brick-red solid. The product exhibited a strong IR stretch at 1751 cm^{-1} and eight inequivalent phosphine methyl resonances in the ^{1}H NMR spectrum, consistent with formation of a six-coordinate carbyne complex.[11,18,30] The coupling of two carbonyl ligands in seven-coordinate tantalum and niobium complexes proceeds via a siloxycarbyne intermediate. For example, [Ta(≡COSiPr$^i_3$)(CO)(dmpe)$_2$] is formed in the reaction of [^{i}Pr$_3$SiCl] with Na[Ta(CO)$_2$(dmpe)$_2$].[11,18] In the cross coupling reaction, two different carbyne intermediates are possible. As shown below, an electrophilic attack might occur at the oxygen

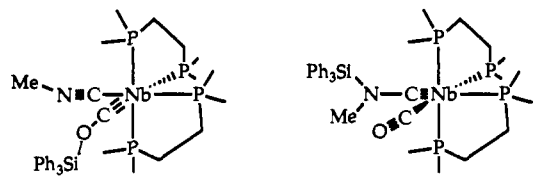

(iv) (v)

atom of the carbonyl to form a siloxycarbyne species (iv) or the silyl reagent could react with the nitrogen atom of the isocyanide ligand yielding a silylaminocarbyne complex (v). To distinguish between these two possibilities, **3a** was prepared from the ^{13}C-labeled complex [Nb(CNMe)(^{13}CO)(dmpe)$_2$Cl]. Since the IR band in ^{13}C-labeled **3a** occurs at 1716 cm^{-1} compared to 1751 cm^{-1} for the unlabeled compound, it must arise from a terminal CO

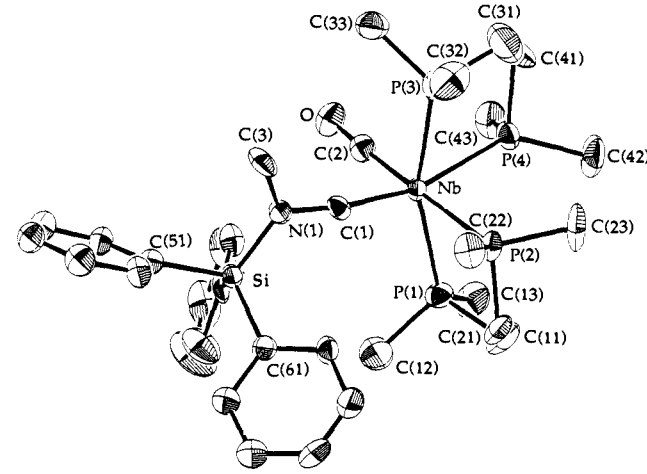

Figure 3. Structure of [Nb{CN(Me)(SiPh$_3$)}(CO)(dmpe)$_2$] (**3a**) showing the 40% probability thermal ellipsoids and the atom labeling scheme. Hydrogen atoms have been omitted.

Table III. Selected Bond Distances (Å) and Angles (deg) for [Nb{CN(Me)(SiPh$_3$)}(CO)(dmpe)$_2$]·$^1/_2$Et$_2$O (**3a**·$^1/_2$Et$_2$O)[a]

Coordination Sphere			
Bond Distances			
Nb–C(1)	1.923 (8)	Nb–P(2)	2.604 (3)
Nb–C(2)	2.04 (1)	Nb–P(3)	2.514 (2)
Nb–P(1)	2.569 (2)	Nb–P(4)	2.661 (3)
Bond Angles			
C(1)–Nb–C(2)	86.6 (5)	C(2)–Nb–P(4)	79.9 (2)
C(1)–Nb–P(1)	101.5 (2)	P(1)–Nb–P(2)	77.1 (1)
C(1)–Nb–P(2)	95.8 (2)	P(1)–Nb–P(3)	162.08 (8)
C(1)–Nb–P(3)	93.7 (2)	P(1)–Nb–P(4)	90.5 (1)
C(1)–Nb–P(4)	163.3 (2)	P(2)–Nb–P(3)	91.5 (1)
C(2)–Nb–P(1)	100.1 (2)	P(2)–Nb–P(4)	98.07 (9)
C(2)–Nb–P(2)	177.0 (2)	P(3)–Nb–P(4)	76.7 (1)
C(2)–Nb–P(3)	90.1 (2)		
Ligand Geometry			
Bond Distances			
C(1)–N(1)	1.38 (1)	N(1)–Si(1)	1.738 (6)
N(1)–C(3)	1.47 (1)	C(2)–O	1.18 (1)
mean Si–C	1.871 (9)	range Si–C	1.86–1.88
mean C–C(aryl)	1.38 (1)	range C–C(aryl)	1.34–1.40
mean P–C	1.85 (1)	range P–C	1.81–1.89
Bond Angles			
C(1)–N(1)–Si	120.4 (5)	Nb–C(1)–N(1)	172.2 (6)
C(1)–N(1)–C(3)	116.4 (6)	Nb–C(2)–O	174.5 (7)
mean N–Si–C	109.0 (4)	range N–Si–C	109–111
mean C–Si–C	108.8 (4)	range C–Si–C	107.1–111.6
mean C–C–C	120 (1)	range C–C–C	117–122
mean C–P–C	100.3 (6)	range C–P–C	98–103

[a] Distances reported have not been corrected for thermal motion. Standard deviations quoted for the mean values are the average of the standard deviations for the individual values. See Figure 3 for atom-labeling scheme.

ligand. Electrophilic attack by Ph$_3$SiCl therefore takes place at the isocyanide rather than the carbonyl group (eq 5).

$$\text{Na[Nb(CNMe)(}^{13}\text{CO)(dmpe)}_2\text{]} \xrightarrow[\text{THF}]{\text{Ph}_3\text{SiCl}} \text{[Nb\{≡CN(Me)(SiPh}_3\text{)\}(}^{13}\text{CO)(dmpe)}_2\text{]} \quad (5)$$

The formulation of **3a** as an aminocarbyne was confirmed by an X-ray diffraction study. Figure 3 displays the structure of **3a**. The niobium geometry (Table III) is distorted octahedral. The amino group containing the atoms N(1), C(1), C(3), and Si is planar and slightly tilted with respect to the P(3)–Nb–P(1) plane. The Nb–C(1) bond distance of 1.923 (8) Å is longer than that found for most carbyne complexes.[38,39] Metal–carbon bonds of

(34) Warnock, G. F.; Cooper, N. J. *Organometallics* **1989**, *8*, 1826.
(35) Warnock, G. F. P.; Sprague, J.; Fjare, K. L.; Ellis, J. E. *J. Am. Chem. Soc.* **1983**, *105*, 672.
(36) Ellis, J. E.; Fjare, K. L. *Organometallics* **1982**, *1*, 898.
(37) Ellis, J. E.; Fjare, K. L. *J. Organomet. Chem.* **1981**, *214*, C33.
(38) Kim, H. P.; Angelici, R. J. In *Adv. Organomet. Chem.* **1987**, *27*, 51.

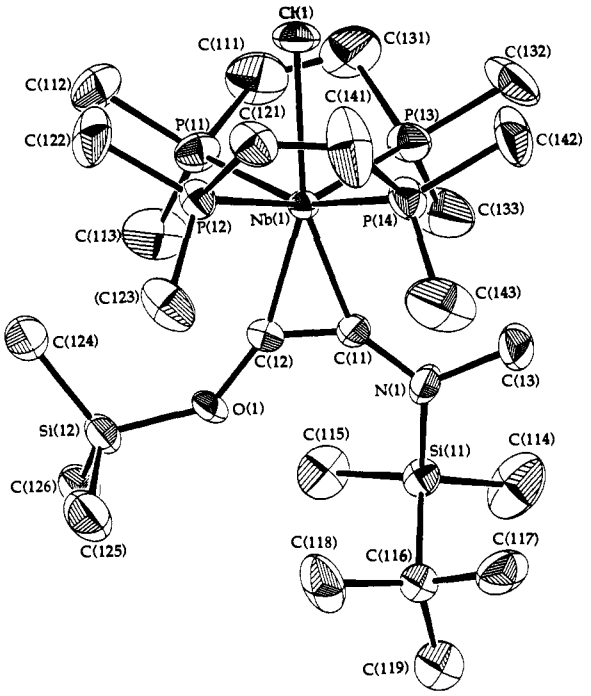

Figure 4. Structure of one of the two independent molecules of [Nb{('BuMe$_2$Si)(Me)NC≡CO(SiMe$_3$)}(dmpe)$_2$Cl] (**4**) showing the 40% probability thermal ellipsoids and the atom labeling scheme. Hydrogen atoms have been omitted.

aminocarbyne complexes are typically longer than those found for alkylidynes, because the π-donating NR_2 group competes with the metal for a carbyne carbon p orbital.[39] In valence bond terms, resonance isomer vii is favored over vi. A more definitive as-

$$\underset{\text{vi}}{L_nM{\equiv}C{-}NR_2} \leftrightarrow \underset{\text{vii}}{{}^{-}L_nM{=}C{=}NR_2{}^{+}}$$

sessment of the metal–carbyne bonding in **3a** is difficult to make because few second row transition metal aminocarbyne complexes have been structurally characterized. The complexes [*mer*-(μ-L)(CO)$_3$Mo≡CNEt$_2$]$_2$ (L = I, NCO) have metal–carbyne bond lengths of ~1.81 Å,[40] and the carbyne M–C distance in the cation [Mo{≡CN(Bu')(SiMe$_2$Bu')}(CNBu')$_5$]$^+$ is 1.866 (9) Å.[17]

Initiation of Aminocarbyne–CO Coupling. The aminocarbyne complex **3a** is stable in the presence of stoichiometric quantities of trimethylsilyl chloride over a period of 12 h. Addition of excess Me$_3$SiCl did not induce coupling, but rather led to oxidation and decomposition. On the supposition that the triphenylsilyl group is too bulky to allow the coupling reaction to proceed, the sterically less demanding 'BuMe$_2$SiCl reagent was employed. Addition of 1 equiv of 'BuMe$_2$SiCl to the anion **2a** caused a color change from dark burgundy to red. Workup yielded [Nb{≡CN(Me)(SiMe$_2$Bu')}(CO)(dmpe)$_2$] (**3b**) as a red-brown oil which could not be further purified. The spectroscopic data for **3b** agree well with that obtained for **3a**, although the IR stretch of the CO ligand was shifted by ~20 cm^{-1} to higher energy. A similar shift has been reported for the related siloxycarbyne species [V(≡COSiR$_3$)(CO)(dmpe)$_2$] (R = Ph, ν_{CO} = 1753 cm^{-1}; R$_3$ = 'BuMe$_2$, ν_{CO} = 1790 cm^{-1}).[30] Two separate resonances were detected in the ^{1}H NMR spectrum for the diastereotopic methyl groups of the 'BuMe$_2$Si functionality. These signals coalesced when the sample was heated above 45 °C, from which the activation energy for racemization at the niobium center can be estimated to be ~67.4 kJ/mol.

Addition of 1 equiv of Me$_3$SiCl to a THF solution of **3b** yielded the asymmetric coupled product [Nb{('BuMe$_2$Si)(Me)NC≡CO(SiMe$_3$)}(dmpe)$_2$Cl] (**4**), as shown in eq 6. Compound **4** exhibited no C≡O or C≡NR stretches in its IR spectrum and did show an acetylenic stretch at 1559 cm^{-1}. The ^{1}H NMR spectrum was similar to that of **1a**, although two resonances for the 'BuMe$_2$Si group were evident, and the ^{31}P{^{1}H} NMR spectrum exhibited a single, broad resonance.

$$\underset{\mathbf{3b}}{[Nb\{CN(Me)(SiMe_2Bu')\}(CO)(dmpe)_2]} \xrightarrow[THF]{Me_3SiCl} \underset{\mathbf{4}}{[Nb\{('BuMe_2Si)(Me)NC{\equiv}CO(SiMe_3)\}(dmpe)_2Cl]} \quad (6)$$

The formation of **4** from **3b** provides direct evidence that aminocarbyne complexes are intermediates in the carbonyl–isocyanide coupling reactions. Although alkylidyne–CO coupling reactions are well precedented,[38,41] the analogous aminocarbyne–CO coupling reactions are rare. In the only other example of such a reaction, addition of CO to [('BuO)$_3$W≡CNR$_2$]$_2$ (R = Me, Et) gave the bridging η^2-iminoketenyl complex, [('BuO)$_3$W(R$_2$NCCO)]$_2$.[33] Carbyne intermediates have also been implicated in the coupling of two isocyanide[17,19,42] and two carbonyl[11,18] ligands. The cross coupling reaction indicates that this series of

Table IV. Selected Bond Distances (Å) and Angles (deg) for [Nb{('BuMe$_2$Si)(Me)NC≡CO(SiMe$_3$)}(dmpe)$_2$Cl][a] (**4**)

Coordination Sphere			
Bond Distances			
Nb(1)–C(11)	2.115 (8)	Nb(2)–C(21)	2.102 (8)
Nb(1)–C(12)	2.080 (7)	Nb(2)–C(22)	2.080 (7)
Nb(1)–Cl(1)	2.589 (2)	Nb(2)–Cl(2)	2.594 (2)
Nb(1)–P(11)	2.552 (2)	Nb(2)–P(21)	2.562 (2)
Nb(1)–P(12)	2.563 (2)	Nb(2)–P(22)	2.570 (2)
Nb(1)–P(13)	2.565 (2)	Nb(2)–P(23)	2.561 (2)
Nb(1)–P(14)	2.558 (2)	Nb(2)–P(24)	2.560 (2)
Bond Angles			
C(11)–Nb(1)–C(12)	36.7 (3)	C(21)–Nb(2)–C(22)	36.1 (3)
Cl(1)–Nb(1)–C(11)	160.9 (2)	Cl(2)–Nb(2)–C(21)	160.9 (2)
Cl(1)–Nb(1)–C(12)	162.3 (2)	Cl(2)–Nb(2)–C(22)	163.0 (2)
mean P–Nb–P$_{chelate}$	75.7 (1)	range P–Nb–P$_{chelate}$	75.3–76.1
mean P–Nb–P$_{cis}$	100.0 (1)	range P–Nb–P$_{cis}$	99.5–100.4
mean P–Nb–P$_{trans}$	157.9 (1)	range P–Nb–P$_{trans}$	156.4–159.6
mean Cl–Nb–P	78.97 (8)	range Cl–Nb–Cl	77.38–80.18
Ligand Geometry			
(i) Acetylene			
Bond Distances			
C(11)–C(12)	1.32 (1)	C(21)–C(22)	1.30 (1)
N(1)–C(11)	1.38 (1)	N(2)–C(21)	1.39 (1)
N(1)–C(13)	1.49 (1)	N(2)–C(23)	1.50 (3)
N(1)–Si(11)	1.807 (9)	N(2)–Si(21)	1.812 (8)
O(1)–C(12)	1.359 (9)	O(2)–C(22)	1.371 (9)
O(1)–Si(12)	1.647 (6)	O(2)–Si(22)	1.643 (6)
mean Si–C	1.85 (2)	range Si–C	1.82–1.94
mean C–C (Bu')	1.61 (2)	range C–C (Bu')	1.57–1.64
Bond Angles			
C(11)–C(12)–O(1)	129.4 (7)	C(21)–C(22)–O(2)	130.4 (7)
C(11)–N(1)–C(13)	116.4 (7)	C(21)–N(2)–C(23)	114 (1)
C(11)–N(1)–Si(11)	125.7 (6)	C(21)–N(2)–Si(21)	124.0 (6)
C(12)–C(11)–N(1)	139.7 (8)	C(22)–C(21)–N(2)	139.5 (7)
C(12)–C(11)–Nb(1)	70.2 (5)	C(22)–C(21)–Nb(2)	71.0 (5)
C(12)–O(1)–Si(12)	141.6 (5)	C(22)–O(2)–Si(22)	139.7 (5)
C(13)–N(1)–Si(11)	115.3 (7)	C(23)–N(2)–Si(21)	121 (1)
N(1)–C(11)–Nb(1)	150.0 (6)	N(2)–C(21)–Nb(2)	149.4 (6)
mean C–Si–C	108.5 (7)	range C–Si–C	103.2–112.1
(ii) 1,2-Bis(dimethylphosphine)ethane			
mean P–C	1.83 (1)	range P–C	1.81–1.87
mean C–P–C	100.3 (6)	range C–P–C	96.3–103.1

[a] Distances reported have not been corrected for thermal motion. Standard deviations quoted for the mean values are the average of the standard deviations for the individual values. See Figure 4 for atom-labeling scheme.

(39) Schubert, U. In *Carbyne Complexes*; Fischer, H., Hofmann, P., Kreissl, F. R., Schrock, R. R., Schubert, U., Weiss, K., Ed.; VCH Publishers: New York, 1988; p 40.

(40) Fischer, E. O.; Wittmann, D.; Himmelreich, D.; Cai, R.; Ackermann, K.; Neugebauer, D. *Chem. Ber.* **1982**, *115*, 3152.

(41) Kreissl, F. R. In *Carbyne Complexes*; Fischer, H., Hofmann, P., Kreissl, F. R., Schrock, R. R., Schubert, U., Weiss, K., Ed.; VCH Publishers: New York, 1988; p 100.

(42) Filippou, A. C.; Grünleitner, W.; Völkl, C.; Kiprof, P. *Angew. Chem., Int. Ed. Engl.* **1991**, *30*, 1167.

reactions provides a general pathway for the construction of functionalized acetylene complexes (Scheme I).

Structure of [Nb{(^{t}BuMe$_2$Si)(Me)NC≡CO(SiMe$_3$)}(dmpe)$_2$Cl] (4). An X-ray crystal structure determination of **4** gave the results shown in Figure 4. The geometry of **4** (Table IV) is very similar to that of **1a**, except that the amino group of the acetylene ligand in **4** is no longer planar. The slight pyramidalization at the nitrogen atom suggests that resonance form iii contributes less than was found in **1a**. The C–C and C–N bond distances of the two structures are very similar, however, and the nonplanarity of the acetylene ligand is more likely the result of intermolecular packing effects.

Formation and Characterization of [TaH(MeHNC≡COH)(dmpe)$_2$Cl]Cl (5). As reported previously,[20] addition of HCl$_{aq}$ to the symmetric CO coupled product [Ta(Me$_3$SiOC≡COSiMe$_3$)(dmpe)$_2$Cl] afforded the first isolated (dihydroxyacetylene)metal complex [TaH(HOC≡COH)(dmpe)$_2$Cl]Cl. A similar reaction with the cross-coupled product **1** was therefore attempted. Addition of 1 equiv of HCl$_{aq}$ to **1b** resulted in a color change from dark green to pale yellow. After workup, a colorless, microcrystalline solid was isolated, the IR spectrum of which showed the characteristic C≡C stretch (1622 cm^{-1}), as well as two bands at 3323 and 3423 cm^{-1}, which arise from the OH and NH stretches. The ^{1}H NMR spectrum revealed a characteristic triplet of triplets at 5.14 ppm, due to a metal hydride, and no resonances that could be attributed to Me$_3$Si groups. The presence of the hydride was further confirmed by the ^{31}P NMR spectrum, which showed P–H coupling of 83 Hz for one of the two observed signals. Finally, the ^{1}H NMR resonance for the *N*-methyl group was split into a doublet, indicating that the nitrogen atom was protonated. Addition of D_2O to the sample caused this doublet to collapse to a singlet. These data are consistent with characterization of **5** as the hydroxy(methylamino)acetylene hydride complex, [TaH(MeHNC≡COH)(dmpe)$_2$Cl]Cl, formed as indicated in eq 7. Addition of more than 1 equiv of HCl$_{aq}$ resulted

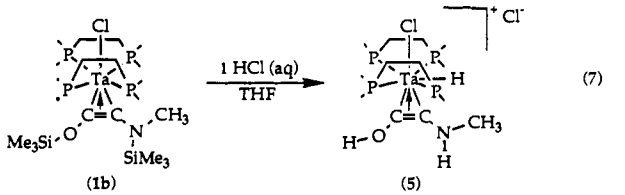

(1b) (5) (7)

in the formation of a white precipitate, which is extremely insoluble and was not further characterized. Analysis of the reaction mixture from the synthesis of **5** by GC–mass spectrometry revealed the presence of Me$_3$SiOH. From these results, we postulate the stoichiometry of the reaction to be that shown in eq 8.

$$\mathbf{1b} + HCl + 2H_2O \rightarrow \mathbf{5} + 2Me_3SiOH \qquad (8)$$

Although short-lived species of the form (HOC≡CNH$_2$) have been detected by mass spectrometry,[43] complex **5** is the first isolated example of the hydroxy(methylamino)acetylene ligand. A single-crystal X-ray structure analysis was therefore carried out to complete the characterization of this interesting compound.

X-ray Crystal Structure of [TaH(MeHNC≡COH)(dmpe)$_2$Cl]Cl·CHCl$_3$ (5·CHCl$_3$). The structure of **5** is shown in Figure 5. The complex has crystallographically-imposed mirror symmetry, with the tantalum atom, acetylene, and chloride ligands lying in the plane. The position of the hydride ligand could not be located from difference Fourier maps. The P(2)–Ta–P(2)* angle of 82.9 (2)° is much smaller than the corresponding P(1)–Ta–P(1)* angle of 124.1 (2)°, however, indicating that the H atom resides between P(1) and P(1)*. The four phosphine ligands and the hydride define the equatorial plane of a pentagonal bipyramid (Table V), with the chloride and midpoint of the acetylene ligand serving as axial ligands. The distance between the oxygen atom of the hydroxy(methylamino)acetylene ligand and the chloride counterion is 3.12 (2) Å, suggesting that a hydrogen bond is formed between the hydroxyl group proton and Cl(2). The N–Cl(2) distance of 3.46 (2) Å is too long for a similar such interaction with the amino group of the coupled ligand.

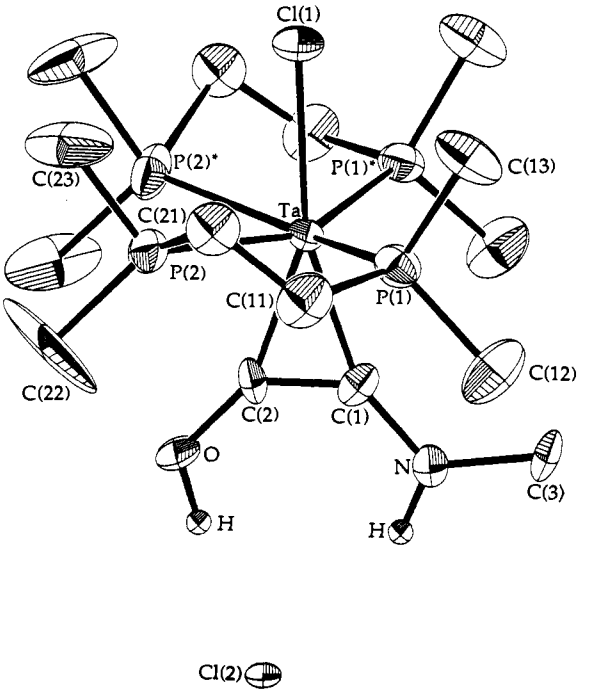

Figure 5. Structure of [TaH(HOC≡CNHMe)(dmpe)$_2$Cl]Cl in the **5**·CHCl$_3$ crystal showing the 40% probability thermal ellipsoids. Hydrogen atoms were generated and have been omitted except for two hydrogen atoms of the acetylene ligand.

Table V. Selected Bond Distances (Å) and Angles (deg) for [Ta(MeHNC≡COH)(dmpe)$_2$Cl]Cl·CHCl$_3$ (**5**·CHCl$_3$)[a]

Coordination Sphere			
Bond Distances			
Ta–C(1)	2.10 (2)	Ta–P(2)	2.630 (5)
Ta–C(2)	2.04 (2)	Ta–Cl(1)	2.542 (6)
Ta–P(1)	2.560 (5)		
Bond Angles			
C(1)–Ta–C(2)	37.2 (9)	C(2)–Ta–Cl(1)	158.9 (7)
C(1)–Ta–P(1)	87.5 (3)	P(1)–Ta–P(1)*	124.1 (2)
C(1)–Ta–P(2)	110.2 (5)	P(1)–Ta–P(2)	155.5 (2)
C(1)–Ta–Cl(1)	163.9 (7)	P(1)–Ta–Cl(1)	84.9 (1)
C(2)–Ta–P(1)	104.4 (3)	P(2)–Ta–P(2)*	82.9 (2)
C(2)–Ta–P(2)	82.7 (5)	P(2)–Ta–Cl(1)	81.5 (2)
Ligand Geometry			
(i) Acetylene			
Bond Distances			
C(1)–C(2)	1.32 (3)	N–C(3)	1.45 (3)
C(1)–N	1.40 (3)	C(2)–O	1.33 (3)
N–Cl(2)	3.46 (2)	O–Cl(2)	3.12 (2)
Bond Angles			
C(1)–C(2)–O	132 (2)	C(2)–C(1)–Ta	73 (1)
C(1)–N–C(3)	125 (2)	N–C(1)–Ta	158 (2)
C(2)–C(1)–N	132 (2)	O–C(2)–Ta	155 (2)
(ii) 1,2-Bis(dimethylphosphine)ethane			
mean P–C	1.83 (4)	range P–C	1.73–2.08
mean C–P–C	102 (2)	range C–P–C	80–121

[a] Distances reported have not been corrected for thermal motion. Standard deviations quoted for the mean values are the average of the standard deviations for the individual values. See Figure 5 for atom-labeling scheme.

Reductive Coupling of Two CNMe Ligands in [Ta(CNMe)$_2$(dmpe)$_2$Cl]. The successful cross coupling of CO with CNR in compounds **2** suggested that the {M(dmpe)$_2$Cl} framework should be capable of supporting the symmetric coupling of two isocyanide ligands. Treatment of a THF solution of [Ta(CNMe)$_2$(dmpe)$_2$Cl] with excess 40% Na/Hg resulted in a color change from burgundy

(43) Terlouw, J. K.; Schwarz, H. *Angew. Chem., Int. Ed. Engl.* **1987**, *26*, 805.

to dark brown. Addition of an excess of Me_3SiCl caused a very slow color change to dark green over a 12-h period. The isolated green product was very soluble in hydrocarbon solvents. It displayed no C≡NR stretches in the IR spectrum but did have a band at 1539 cm^{-1}, characteristic of the C–C acetylene stretch observed for the dicarbonyl and mixed CO/CNR coupled products. The $^{31}P\{^1H\}$ NMR spectrum exhibited a single, broad resonance indicating a symmetric arrangement of the dmpe ligands. Finally, the ^1H NMR showed single N–Me and $SiMe_3$ resonances and two PCH_3 and PCH_2 signals consistent with the coupled species, $[Ta\{(Me_3Si)(Me)NC{\equiv}CN(Me)(SiMe_3)\}(dmpe)_2Cl]$ (**6**) (eq 9).

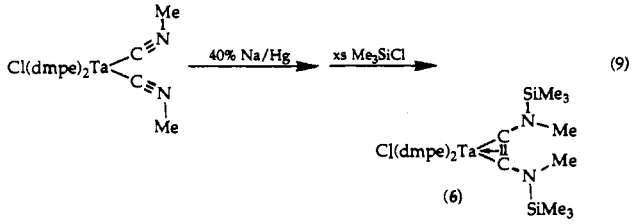

(9)

No attempt has been made to isolate or identify intermediates in this reaction, but sufficient precedent now exists that we can presume with some confidence that it proceeds by sequence of steps shown in Scheme I. Reduction of $[Ta(CNMe)_2(dmpe)_2Cl]$ should generate the tantalum(–I) anion, $[Ta(CNMe)_2(dmpe)_2]^-$, which, when allowed to react with Me_3SiCl, should afford the aminocarbyne complex, $[Ta\{CN(Me)(SiMe_3)\}(CNMe)(dmpe)_2]$. The slow rate of the coupling step may be the result of unfavorable steric interactions between the two methyl groups of the substituted acetylene ligand in **6**. This ligand would most likely be strongly distorted from planarity. X-ray quality crystals of this species could not be obtained, however, so this suggesion has not been evaluated.

Conclusions

Reductive coupling of CO and CNR ligands by low-valent group V transition metals has now been achieved in all combinations. In addition to the previously reported ($Me_3SiOC{\equiv}COSiMe_3$) and (HOC≡COH) moieties, three new highly functionalized acetylene ligands have been formed by reductive coupling reactions, as shown below. The cross coupling of CO and

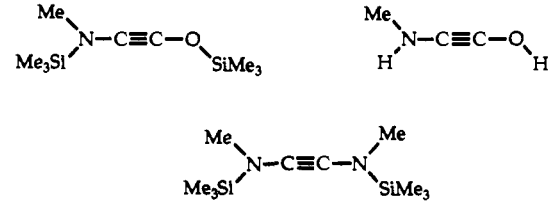

CNMe ligands proceeds by a mechanism analogous to that previously reported for the symmetric carbon monoxide and isocyanide reductive coupling reactions. Aminocarbyne intermediates were isolated, one of which has been crystallographically characterized. Addition of Me_3SiCl to $[Nb\{CN(Me)(SiMe_2Bu^t)\}(CO)(dmpe)_2]$ generated the asymmetric coupled product $[Nb\{(^tBuMe_2Si)(Me)(NC{\equiv}CO(SiMe_3)\}(dmpe)_2Cl]$, demonstrating that these aminocarbyne complexes are on the reductive coupling reaction pathway. Addition of aqueous acid to $[Ta\{(Me_3Si)OC{\equiv}CN(Me)(SiMe_3)\}(dmpe)_2Cl]$ provided the first stabilized hydroxy(alkylamino)acetylene complex, $[TaH(HOC{\equiv}CNHMe)(dmpe)_2Cl]Cl$. Finally, reductive coupling of two isocyanide ligands in $[Ta(CNMe)_2(dmpe)_2Cl]$ has been accomplished, demonstrating that all three combinations of CO and CNR ligands can be linked by reductive coupling reactions using the same metal framework.

Acknowledgment. This work was supported by a grant from the National Science Foundation.

Supplementary Material Available: Atomic positions and thermal parameters for all crystallographically characterized compounds (17 pages); tables of observed and calculated structure factors for all crystallographically characterized compounds (140 pages). Ordering information is given on any current masthead page.

Mechanism of Equilibration of Diastereomeric Chiral Rhenium Alkene Complexes of the Formula $[(\eta^5\text{-}C_5H_5)Re(NO)(PPh_3)(H_2C{=}CHR)]^+BF_4^-$. The Metal Traverses between Alkene Enantiofaces without Dissociation!

Tang-Sheng Peng and J. A. Gladysz*

Contribution from the Department of Chemistry, University of Utah, Salt Lake City, Utah 84112.
Received December 5, 1991

Abstract: The (*RS,SR*)/(*RR,SS*) diastereomers of $[(\eta^5\text{-}C_5H_5)Re(NO)(PPh_3)(H_2C{=}CHR)]^+BF_4^-$ (**1**: R = (**a**) CH_3, (**b**) $CH_2CH_2CH_3$, (**c**) $CH_2C_6H_5$, (**d**) C_6H_5, (**e**) $CH(CH_3)_2$, (**g**) $Si(CH_3)_3$) differ in the alkene enantioface bound to rhenium, and interconvert in chlorocarbons at 95–100 °C. Isomerization is nondissociative (no incorporation of deuterated alkenes or PPh_3) and occurs with retention of configuration at rhenium and without scrambling of *E*/*Z* deuterium labels. The latter excludes mechanisms that involve intermediate carbocations $ReCH_2CHR^+$ and alkylidene complexes, and nucleophilic addition to the alkene. The isomerization of (*RR,SS*)-**1d** to (*RS,SR*)-**1d** proceeds (96.5 °C) with $k(H)/k(=CHD_E) = 1.64$, $k(H)/k(=CHD_Z) = 1.07$, and $k(H)/k(=CDC_6H_5) = 1.15$. Triethylamine promotes the isomerization of substrates that bear allylic protons via σ-allyl complexes $(\eta^5\text{-}C_5H_5)Re(NO)(PPh_3)(CH_2CH{=}CHR')$. However, rate data suggest that "conducted tour" mechanisms involving transient binding to *RC*=C substituents are unlikely. These results are best accommodated by a mechanism in which the rhenium moves through the π nodal plane of the alkene via a carbon–hydrogen "σ bond complex" involving H_E and/or a vinyl hydride oxidative addition product.

Chiral transition-metal reagents and catalysts are now extensively utilized for the elaboration of achiral alkenes to optically active organic molecules.[1] When the substrate alkenes coordinate to chiral metal fragments, two π diastereomers are possible. These

0002-7863/92/1514-4174$03.00/0